energies

Article

Implementation of a Parallel-Series Resonant Converter with Wide Input Voltage Range

Bor-Ren Lin

Department. of Electrical Engineering, National Yunlin University of Science and Technology, Yunlin 640, Taiwan; linbr@yuntech.edu.tw; Tel.: +886-912312281

Received: 8 October 2019; Accepted: 25 October 2019; Published: 26 October 2019

Abstract: A new resonant converter is presented to have the advantages of soft switching operation on power devices, without reverse recovery current loss on power diodes and wide input voltage range operation. Resonant converter with frequency modulation is adopted in the proposed circuit to accomplish the low switching loss on power switches and possible zero current switching operation on fast recovery diodes. To improve the problem of limit voltage range operation in the conventional resonant converter, a new parallel-series structure resonant converter is studied to achieve wide input voltage operation capability, such as from $V_{in,min}$ to $4V_{in,min}$. A 1.8 kW laboratory circuit is implemented, and the measured results are provided to confirm the theoretical analysis and circuit performance.

Keywords: soft switching; reverse recovery current loss; wide input voltage operation

1. Introduction

Modern power converters with high efficiency and high power density are important to achieve compact size and low power loss. To achieve the low switching loss and compact size, the soft switching circuit topologies with the high switching frequency using wide-band gap power devices, such as GaN power devices, have been developed in modern power electronics. The GaN devices have low switching loss characteristic at high switching frequency, so that the converter efficiency is increased. The main drawback of GaN power devices is high cost compared to power MOSFETs. For the past twenty years, the quasi-resonant (QR) flyback converter [1,2] with low turn-on switching loss, the active clamp dc/dc converters [3] with zero voltage switching operation, the resonant converters [4–6] with soft switching operation on power semiconductors, and pulse width modulation (PWM) converters [7–9] have been developed to implement high efficiency converters with power MOSFETs devices. QR flyback [1,2] is limited at low power applications, and active clamp dc/dc converters [3] have the problems of dc magnetizing current and unbalance voltage and current stresses on the rectifier diodes. For conventional resonant converters [4–6], the input voltage variation is limited due to the limited available voltage gain on the resonant tank. Conventional phase-shift PWM full bridge converters [7–9] have drawbacks of hard switching loss at light or low load condition, and high freewheeling current at low load or high input voltage condition. For solar photovoltaic systems, the output voltage of a solar panel is relative to geographical location and solar intensity, so that the solar cell panel has wide output voltage range. Therefore, the power converters with wide voltage operation and high circuit efficiency are demanded for solar power systems. The dc/dc converters with the widespread voltage operation have been proposed in [10–15] for fuel cell and solar power converters. In [10,11], the series-connected or parallel-connected structure has been studied to achieve wide input voltage operation on fuel cell power conversion. In [12–15], the phase-shift PWM dc/dc power converters have been presented to achieve wide voltage operation. In [16], the full-bridge resonant converter with one ac switch and two transformers is proposed to achieve wide input voltage operation. The main drawbacks in [16] are (1) transformer will be shorted suddenly when ac switch is turned on, which will result in serious problems at the transient voltage change and make system unstable, (2) the control scheme of this circuit topology is much more complicated with four equivalent operation topologies, and (3) some power switches will always be conducting at some specific circuit topologies that will increase the conduction loss.

A new parallel-series (full bridge resonant converters are parallel connection and diode rectifiers are series connection) based resonant circuit is developed to obtain the main benefits of the wide input voltage range operation (from $v_{in,min}$ to $4V_{in,min}$) and soft switching operation on power semiconductors. The variable frequency control is used to regulate load voltage over wide input voltage variation. The input impedance of the equivalent resonant tank in the proposed power converter is controlled under the inductive load characteristic. Therefore, the soft switching operation on power semiconductors is achieved. Since two diode rectifiers of the proposed converter are series-connected on the secondary sides, two resonant converters with the parallel-connection on the primary side are worked at the low voltage input (from 100 V to 200 V) to have high dc voltage gain. For high input voltage range (from 200 V to 400 V), only one resonant converter is operated on the primary side to reduce the conduction loss and obtain low dc voltage gain. Therefore, the developed resonant converter can be operated from V_{in} = 100 V to 400 V. At the low input voltage range, the parallel-series based resonant converter can provide 1.8 kW to output load. At the high input voltage range, only one resonant tank is operated (the other resonant tank is off) to provide 1 kW to output load. The main advantages of the proposed converter compared to [16] are a simple control scheme and low current rating of power switches. At the high input voltage, only four switches instead of eight power switches are operated to reduce power conduction losses. At the low input voltage range, eight power switches are operated to achieve high voltage gain and reduce current rating on each power switch for more power output. The circuit structure, the principle of operation, and design procedure are provided and discussed in this paper. Finally, the experimental waveforms with a 1.8 kW laboratory circuit are presented to show the theoretical examination and investigation of wide input voltage capability.

2. Circuit Diagram and Operating Principle

Figure 1a illustrates the presented resonant converter with wide input voltage operation. Two resonant converters are used in the studied circuit with parallel-series connection. V_{in} is the input voltage and V_o is the output voltage. L_{r1} and L_{r2} are resonant inductors, C_{r1} and C_{r2} are resonant capacitors, and L_{m1} and L_{m2} are the magnetizing inductors of transformers T_1 and T_2, respectively. In each resonant circuit, the primary side is a full bridge power converter for medium power rating, and the output side is a full-wave diode rectifier. The passive components (C_{r1} and L_{r1}) and (C_{r2} and L_{r2}) are naturally resonant in each resonant tank to allow the soft switching on power switches. In low input voltage range V_{in} = 100 V ~ 200 V (Figure 1b), two resonant converters are operated with primary-parallel and secondary-series structure. Each resonant converter provides power P to output load. Therefore, the total output power is $2P$. Due to the series connection of two diode rectifiers, the load voltage V_o is the sum of two rectified voltages. Therefore, the voltage rating of diodes D_1 ~ D_8 equals $V_o/2$. The voltage gain G_{each} of each resonant circuit is controlled between 1 and 2. Therefore, the total voltage gain G_{Total} of the studied circuit operating at parallel-series connection is regulated at G_{Total} = 2 ~ 4 under the low input voltage range from V_{in} = 100 V ~ 200 V and V_o = 400 V. In the high input voltage operation (V_{in} = 200 V~400 V) as shown in Figure 1c, only one resonant converter (Q_1 ~ Q_4) is operated, and the other resonant converter (Q_5 ~ Q_8) is off. The diodes D_5 ~ D_8 are all conducting, and V_o equals the average rectified voltage of the diode rectifier by D_1 ~ D_4. Since the voltage gain of resonant circuit is controlled at G_{Total} = 1 ~ 2, the output voltage V_o can be regulated at 400 V under high input voltage range from V_{in} = 200 V ~ 400 V. Based on the circuit structures shown in Figure 1b,c for low and high voltage input, the wide input voltage operation and the soft switching characteristics are accomplished in the proposed power circuit.

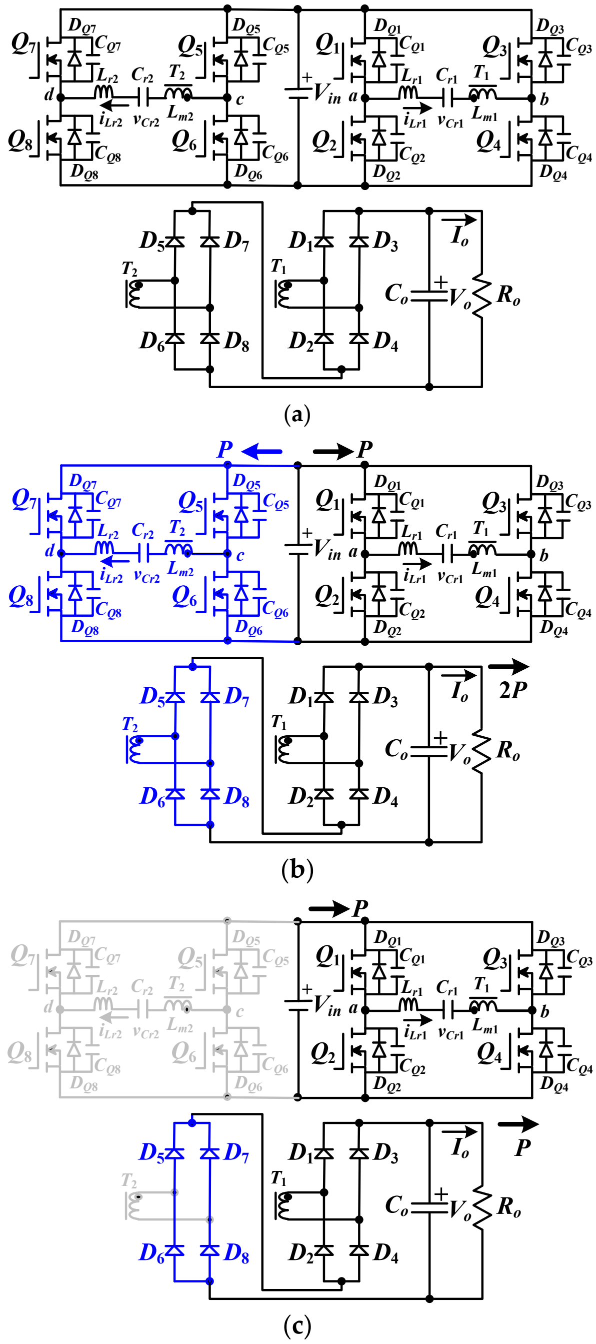

Figure 1. Circuit configurations of the developed dc/dc converter: (**a**) The proposed circuit structure; (**b**) at low voltage input range; (**c**) at high voltage input range.

2.1. Under Low Voltage Input Range (V_{in} = 100 V ~ 200 V)

For low voltage input range, two resonant circuits with parallel-series connection are operated to achieve the higher voltage gain. The dc voltage gain of each resonant converter is controlled between 1 and 2. Since two rectified voltages on the secondary-side are series-connected, the resultant voltage gain of the proposed parallel-series connected resonant converter is regulated between 2 and 4 under 100 V < V_{in} < 200 V. The proposed converter has six operating steps in every switching cycle. Under the condition of f_s (switching frequency) > f_r (resonant frequency), the main PWM waveforms are demonstrated in Figure 2a. The equivalent circuits of six operating steps are provided in Figure 2b–g.

Step 1 [t_0 ~ t_1]: D_1, D_4, D_5, and D_8 are conducting at t_0. Since Q_1, Q_4, Q_5, and Q_8 are conducting, the voltages $v_{ab} = v_{cd} = V_{in}$ and $v_{Lm1} = v_{Lm2} = nV_o$, where n is the turns ratio of T_1 and T_2. Components C_{r1} and L_{r1} are naturally resonant in the first resonant converter, and components C_{r2} and L_{r2} are also naturally resonant in the second resonant converter. The resonant frequency $f_r = 1/2\pi\sqrt{L_{r1}C_{r1}}$.

Step 2 [t_1 ~ t_2]: Q_1, Q_4, Q_5, and Q_8 turn off at time t_1. i_{Lr1} and i_{Lr2} are positive. Thus, C_{Q2}, C_{Q3}, C_{Q6}, and C_{Q7} are discharged, and C_{Q1}, C_{Q4}, C_{Q5}, and C_{Q8} are charged in this step. Due to $i_{Lr1} > i_{Lm1}$ and $i_{Lr2} > i_{Lm2}$, D_1, D_4, D_5, and D_8 are conducting.

Step 3 [t_2 ~ t_3]: At t_2, the voltages of C_{Q2}, C_{Q3}, C_{Q6}, and C_{Q7} are decreased to zero voltage. Since i_{Lr1} and i_{Lr2} are still positive, D_{Q2}, D_{Q3}, D_{Q6}, and D_{Q7} conduct. Thus, Q_2, Q_3, Q_6, and Q_7 can turn on after t_2 with soft switching operation. Since $i_{Lr1} > i_{Lm1}$ and $i_{Lr2} > i_{Lm2}$, diodes D_1 and D_4 in the first diode rectifier and D_5 and D_8 in the second diode rectifier are forward biased. Owing to $v_{ab} = v_{cd} = -V_{in}$ and $v_{Lm1} = v_{Lm2} = nV_o$, i_{Lr1} and i_{Lr2} are decreased, and i_{Lm1} and i_{Lm2} are increased.

Step 4 [t_3 ~ t_4]: At time t_3, i_{Lr1} is less than i_{Lm1}, and i_{Lr2} is less than i_{Lm2}. D_2, D_3, D_6, and D_7 are conducting. The magnetizing voltages v_{Lm1} and v_{Lm2} are $-nV_o$ so that i_{Lm1} and i_{Lm2} are decreased. L_{r1} and C_{r1} are naturally resonant with resonant frequency $f_r = 1/2\pi\sqrt{L_{r1}C_{r1}}$ in the first resonant converter. Similarly, L_{r2} and C_{r2} are naturally resonant in the second resonant converter.

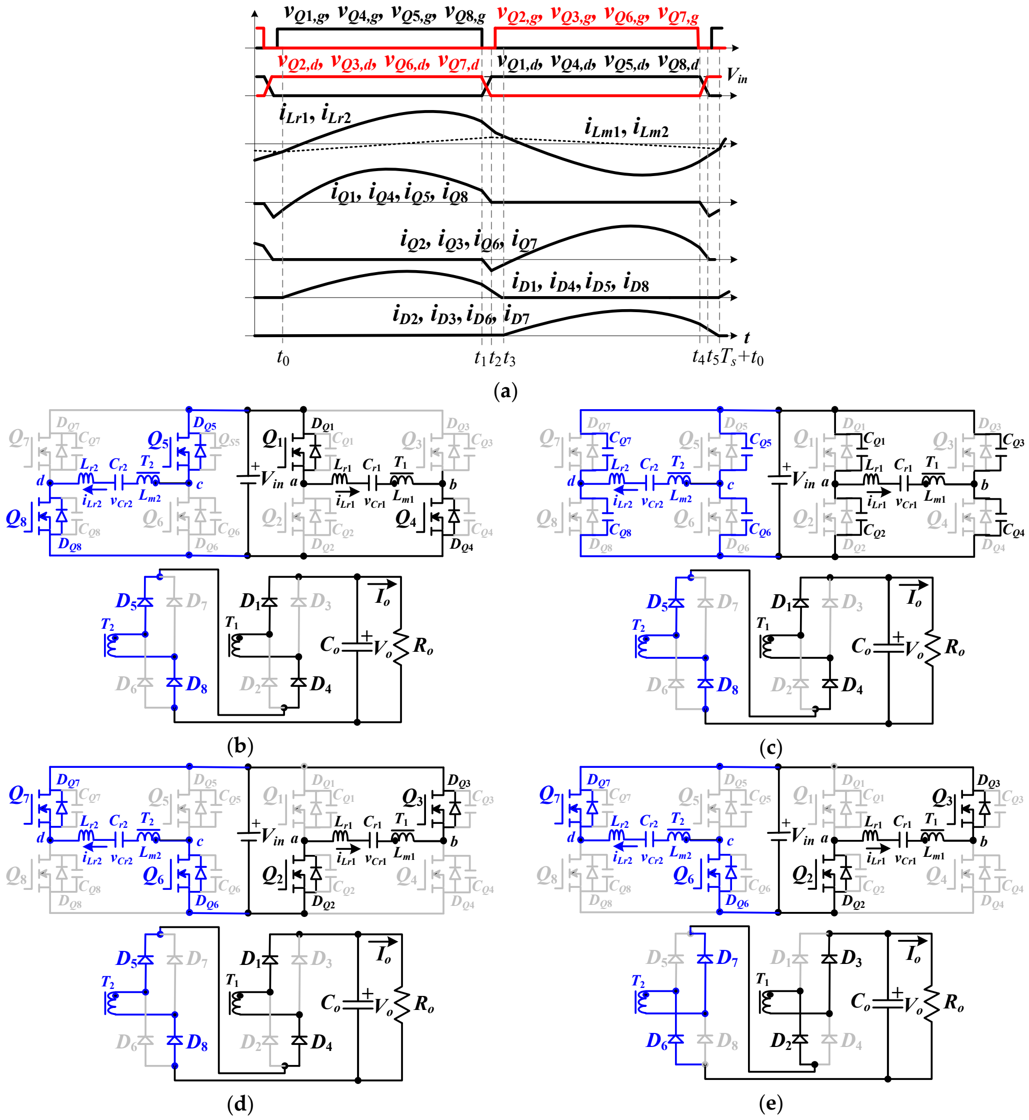

Figure 2. *Cont.*

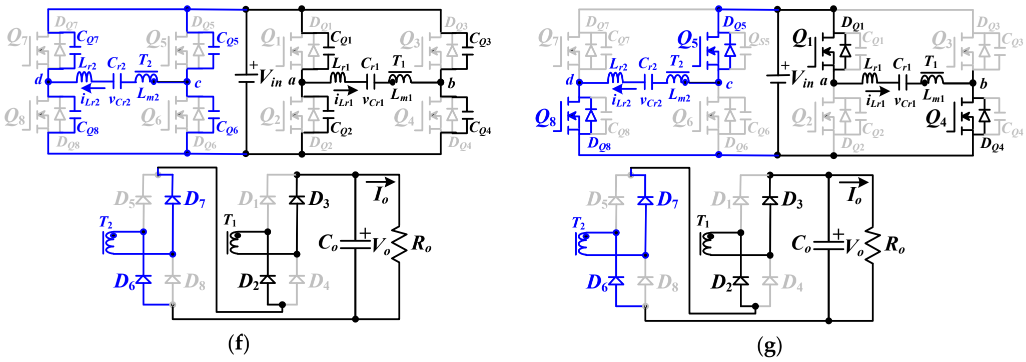

Figure 2. Circuit waveforms and equivalent circuits at low input voltage range and $f_s > f_r$, (**a**) PWM waveforms, (**b**) step 1, (**c**) step 2, (**d**) step 3, (**e**) step 4, (**f**) step 5, (**g**) step 6.

Step 5 [t_4 ~ t_5]: At t_4, switches Q_2, Q_3, Q_6, and Q_7 turn off. Owing to $i_{Lr1} < 0$ and $i_{Lr2} < 0$, C_{Q1}, C_{Q4}, C_{Q5}, and C_{Q8} are discharged and C_{Q2}, C_{Q3}, C_{Q6} and C_{Q7} are charged in step 5. In this step, $i_{Lr1} < i_{Lm1}$ and $i_{Lr2} < i_{Lm2}$ so that D_2, D_3, D_6, and D_7 are conducting.

Step 6 [t_5 ~ T_s+t_0]: At time t_5, the capacitor voltages of C_{Q1}, C_{Q4}, C_{Q5}, and C_{Q8} are decreased to zero voltage. Owing to $i_{Lr1} < 0$ and $i_{Lr2} < 0$, D_{Q1}, D_{Q4}, D_{Q5}, and D_{Q8} conduct. Therefore, Q_1, Q_4, Q_5, and Q_8 turn on after t_5 with soft switching operation. Since $i_{Lr1} < i_{Lm1}$ and $i_{Lr2} < i_{Lm2}$, D_2, D_3, D_6, and D_7 are still conducting. Owing to $v_{ab} = v_{cd} = V_{in}$ and $v_{Lm1} = v_{Lm2} = -nV_o$, the primary side currents i_{Lr1} and i_{Lr2} are increased, and i_{Lm1} and i_{Lm2} are decreased. At time $T_s + t_0$, $i_{Lr1} > i_{Lm1}$, and $i_{Lr2} > i_{Lm2}$ so that D_1, D_4, D_5, and D_8 conduct.

The main PWM waveforms and the equivalent step circuits at low voltage input range under $f_s < f_r$ condition are provided in Figure 3. Under this condition, the presented circuit has six operation steps in every switching cycle. The circuit operations at $f_s < f_r$ condition are discussed as follows.

Step 1 [t_0 ~ t_1]: $v_{CQ1} = v_{CQ4} = v_{CQ5} = v_{CQ8} = 0$ at time t_0. Owing to $i_{Lr1}(t_0)$ and $i_{Lr2}(t_0)$ are negative, diodes D_{Q1}, D_{Q4}, D_{Q5}, and D_{Q8} are conducting. Q_1, Q_4, Q_5, and Q_8 can turn on after t_0 with soft switching operation. In step 1, $v_{ab} = v_{cd} = V_{in}$ and $v_{Lm1} = v_{Lm2} = nV_o$. C_{r1} and L_{r1} are naturally resonant in the first resonant tank, and C_{r2} and L_{r2} are naturally resonant in the second resonant tank.

Step 2 [t_1 ~ t_2]: Since $f_s < f_r$, i_{Lr1} and i_{Lr2} will equal i_{Lm1} and i_{Lm2} at time t_1 and D_1 ~ D_8 are reverse biased. On the primary-side, L_{r1}, L_{m1}, and C_{r1} are naturally resonant in the first resonant converter and L_{r2}, L_{m2}, and C_{r2} are naturally resonant in the second resonant converter.

Step 3 [t_2 ~ t_3]: Q_1, Q_4, Q_5, and Q_8 are turned off at time t_2. C_{Q2}, C_{Q3}, C_{Q6}, and C_{Q7} are discharged due to $i_{Lr1}(t_2)$ and $i_{Lr2}(t_2)$ are both positive. Since the secondary-side currents of T_1 and T_2 are negative, D_2, D_3, D_6, and D_7 are forward biased. If the energy on L_{r1}, L_{r1}, L_{m1}, and L_{m2} at time t_2 is large enough, then the voltages of C_{Q2}, C_{Q3}, C_{Q6}, and C_{Q7} can decrease to zero at time t_3. The soft switching condition of power switches Q_2, Q_3, Q_6, and Q_7 are expressed as.

$$i_{Lm1}(t_2) = i_{Lm2}(t_2) = nV_o/(4L_m f_s) \geq V_{in}\sqrt{4C_e/(L_m + L_r)}, \tag{1}$$

where $L_m = L_{m1} = L_{m2}$, $C_e = C_{Q1} = \ldots = C_{Q8}$ and $L_r = L_{r1} = L_{r2}$.

Step 4 [t_3 ~ t_4]: At time t_3, $v_{CQ2} = v_{CQ3} = v_{CQ6} = v_{CQ7} = 0$. Since $i_{Lr1}(t_3)$ and $i_{Lr2}(t_3)$ are positive, D_{Q2}, D_{Q3}, D_{Q6}, and D_{Q7} are conducting. Then Q_2, Q_3, Q_6, and Q_7 can turn on after time t_3 with zero-voltage switching. In this step, components C_{r1} and L_{r1} are naturally resonant in the first resonant tank and C_{r2} and L_{r2} are naturally resonant in the second resonant tank.

Step 5 [t_4 ~ t_5]: At time t_4, i_{Lm1} equals i_{Lr1} and i_{Lm2} equals i_{Lr2}. Thus, D_1 ~ D_8 are all reverse biased. In the first converter, L_{r1}, L_{m1}, and C_{r1} are resonant, and L_{r2}, L_{m2}, and C_{r2} are naturally resonant in the second converter with input voltage $v_{ab} = v_{cd} = -V_{in}$.

Step 6 [t_5 ~T_s + t_0]: Q_2, Q_3, Q_6, and Q_7 turn off at t_5. Since $i_{Lr1}(t_5)$ and $i_{Lr2}(t_5)$ are negative, C_{Q1}, C_{Q4}, C_{Q5}, and C_{Q8} are discharged from t_5. At time T_s + t_0, v_{CQ1}, v_{CQ4}, v_{CQ5}, and v_{CQ8} are decreased to zero voltage.

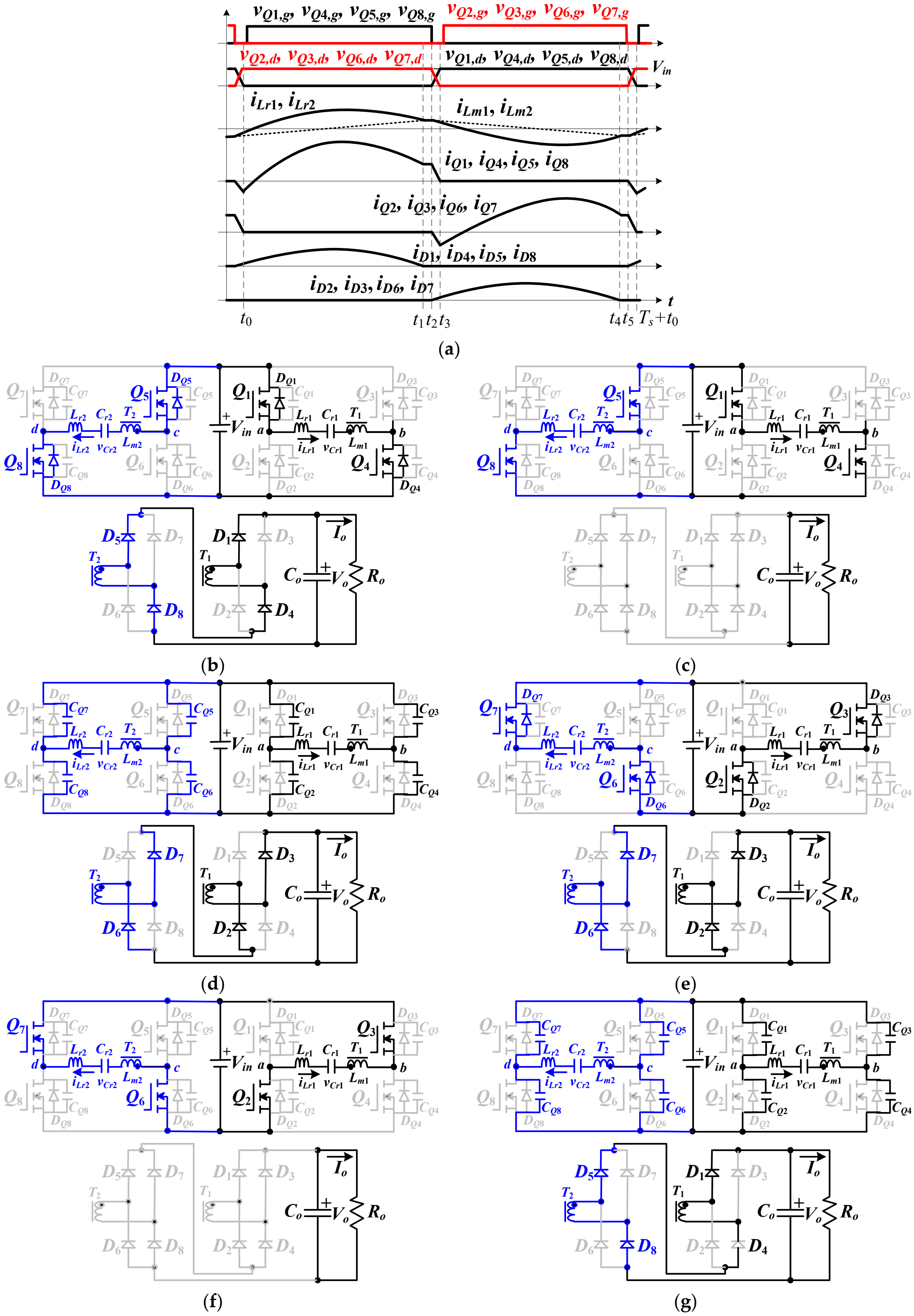

Figure 3. Circuit waveforms and equivalent circuits at low input voltage range and $f_s < f_r$, (**a**) PWM waveforms, (**b**) step 1, (**c**) step 2, (**d**) step 3, (**e**) step 4, (**f**) step 5, (**g**) step 6.

2.2. Under High Voltage Input Range (V_{in} = 200 V ~ 400 V)

For high input voltage case, only one resonant converter (Q_1 ~ Q_4) is operated and the other resonant converter (Q_5 ~ Q_8) is off. The rectifier diodes D_5 ~ D_8 are all conducting and the output voltage of T_1 is connected to the output load (Figure 1c). The voltage gain of the proposed resonant converter is regulated between 1 and 2 under 200 V < V_{in} < 400 V. The proposed converter under high voltage input case has six operating steps for every switching cycle. Figure 4a gives the PWM waveforms under the condition of $f_s > f_r$. Figure 4b–g demonstrate the equivalent circuits of six operating steps. The circuit operations under high input voltage range and $f_s > f_r$ are presented below.

Step 1 [t_0 ~ t_1]: D_1 and D_4 are conducting after time t_0. Since Q_1, Q_4, D_1, D_4, and D_5 ~ D_8 are conducting, it can obtain the voltages $v_{ab} = V_{in}$ and $v_{Lm1} = nV_o$. Components C_{r1} and L_{r1} are resonant.

Step 2 [t_1 ~ t_2]: Q_1 and Q_4 turn off at t_1. Due to $i_{Lr1}(t_1)$ is positive, C_{Q2} and C_{Q3} are charged. Owing to $i_{Lr1}(t_1) > i_{Lm1}(t_1)$, D_1, D_4, and D_5 ~ D_8 are conducting.

Step 3 [t_2 ~ t_3]: At time t_2, $v_{CQ2} = v_{CQ3} = 0$. Since $i_{Lr1}(t_2) > 0$, D_{Q2} and D_{Q3} are forward biased and Q_2 and Q_3 turn on at zero voltage after t_2. Since $i_{Lr1}(t_2) > i_{Lm1}(t_2)$, D_1, D_4, and D_5 ~ D_8 conduct. In this step, $v_{ab} = -V_{in}$ and $v_{Lm1} = nV_o$ so that i_{Lr1} decreases and i_{Lm1} increases.

Step 4 [t_3 ~ t_4]: At t_3, $i_{Lr1} < i_{Lm1}$, and D_2 and D_3 are conducting. In step 4, $v_{Lm1} = -nV_o$ and i_{Lm1} decreases. C_{r1} and L_{r1} are naturally resonant with resonant frequency $f_r = 1/2\pi\sqrt{L_{r1}C_{r1}}$.

Step 5 [t_4 ~ t_5]: At t_4, Q_2 and Q_3 are turned off. Since $i_{Lr1}(t_4) < 0$, C_{Q1} and C_{Q4} are discharged. In this step, $i_{Lr1} < i_{Lm1}$ so that D_2, D_3, and D_6 ~ D_8 are conducting.

Step 6 [t_5 ~ T_s+t_0]: At time t_5, $v_{CQ1} = v_{CQ4} = 0$. Since $i_{Lr1}(t_5) < 0$, D_{Q1} and D_{Q4} are conducting and Q_1 and Q_4 turn on at zero voltage after t_5. Owing to $i_{Lr1} < i_{Lm1}$, D_2, D_3, and D_6 ~ D_8 are conducting. In this step, $v_{ab} = V_{in}$ and $v_{Lm1} = -nV_o$ so that i_{Lr1} increases and i_{Lm1} decreases. At time T_s+t_0, $i_{Lr1} > i_{Lm1}$. Then, D_1, D_4, and D_5 ~ D_8 are conducting.

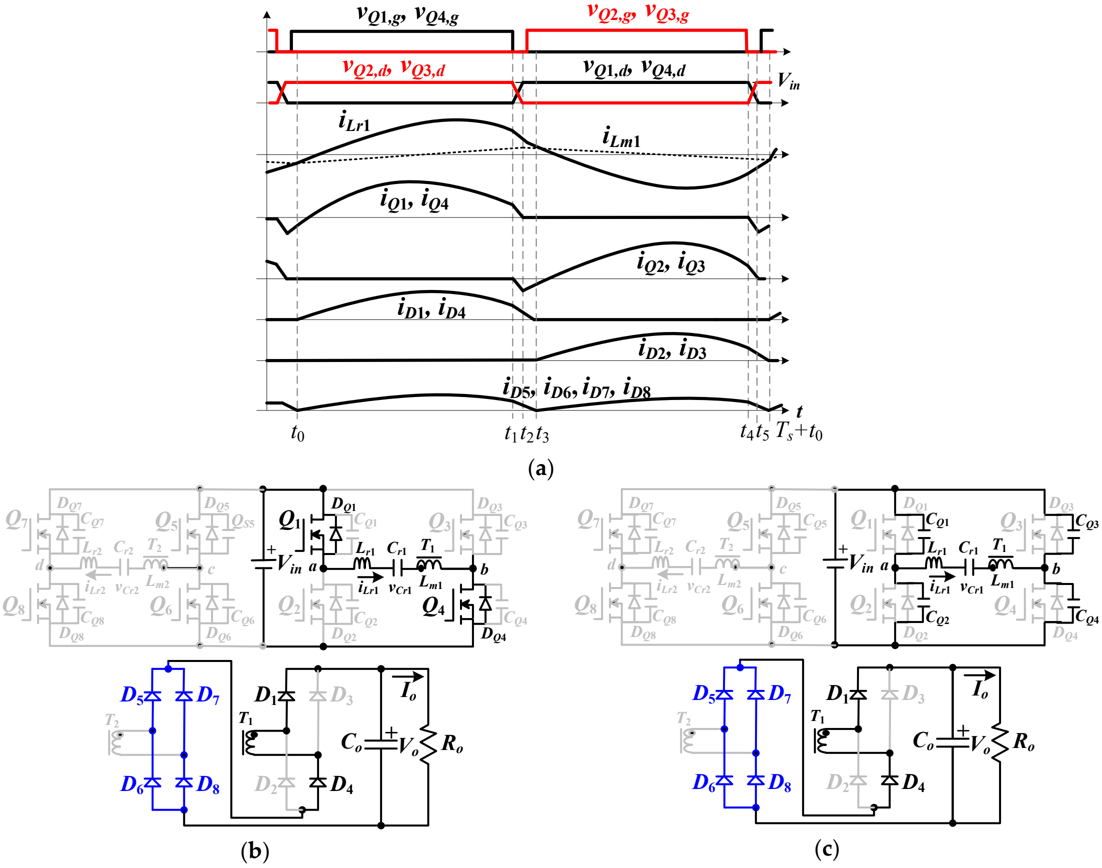

Figure 4. *Cont.*

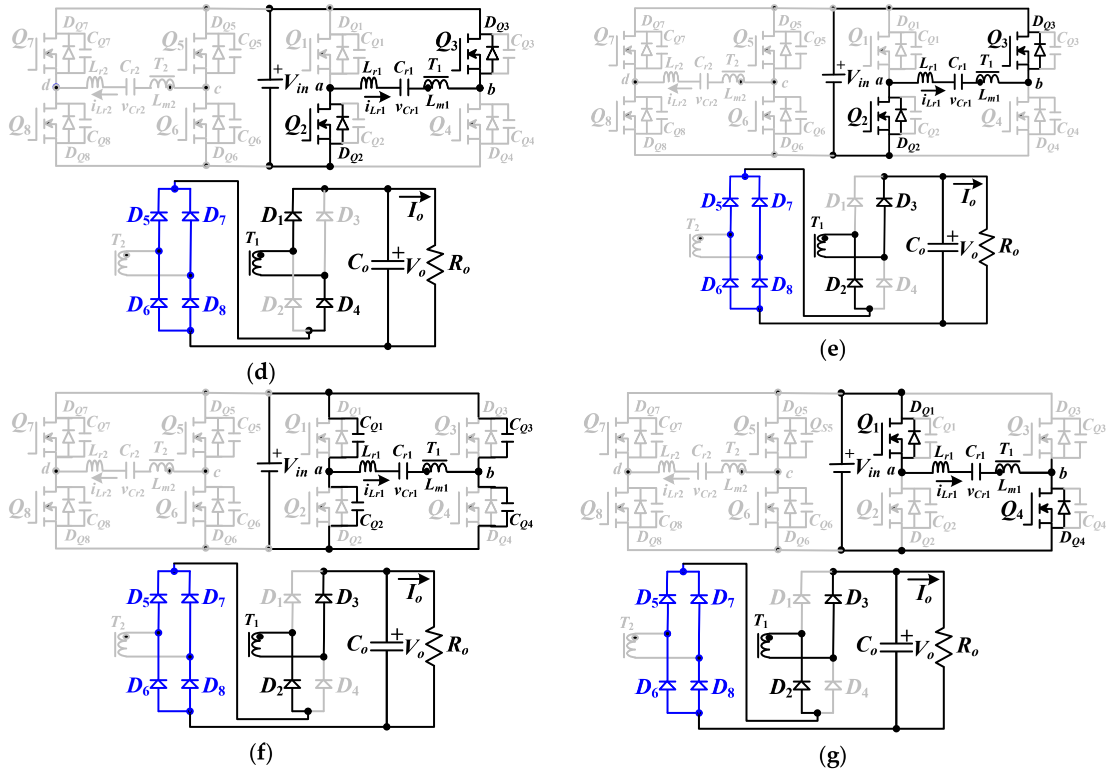

Figure 4. Circuit waveforms and equivalent circuits at high input voltage range and $f_s > f_r$, (**a**) PWM waveforms, (**b**) step 1, (**c**) step 2, (**d**) step 3, (**e**) step 4, (**f**) step 5, (**g**) step 6.

The PWM waveforms under $f_s < f_r$ condition are given in Figure 5a and the equivalent circuits in every cycle under high voltage input range are provided in Figure 5b–g. The operation principles under high voltage input and $f_s < f_r$ condition are discussed as follows.

Step 1 [t_0 ~ t_1]: When $t < t_0$, Q_1 ~ Q_4 are all off and C_{Q1} and C_{Q4} are discharged due to $i_{Lr1} < 0$. At time t_0, $v_{CQ1} = v_{CQ4} = 0$, and D_{Q1} and D_{Q4} are conducting. Thus, Q_1 and Q_4 can turn on after t_0 with soft switching operation. The load current flows through the components D_1, C_o, R_o, D_5 ~ D_8, and D_4 so that the magnetizing inductor voltage $v_{Lm1} = nV_o$ and i_{Lm1} increases. C_{r1} and L_{r1} are naturally resonant with $v_{ab} = V_{in}$ and $v_{Lm1} = nV_o$.

Step 2 [t_1 ~ t_2]: At t_1, $i_{Lm1} = i_{Lr1}$ and D_1 ~ D_8 are all off. L_{r1}, L_{m1}, and C_{r1} are naturally resonant with $V_{ab} = V_{in}$.

Step 3 [t_2 ~ t_3]: At t_2, Q_1, and Q_4 turn off. Owing to $i_{Lr1}(t_2) > 0$, C_{Q2} and C_{Q3} are discharged. Since $i_{Lr1} < i_{Lm1}$ after t_2, D_2, D_3, and D_5 ~ D_8 conduct.

Step 4 [t_3 ~ t_4]: At $t = t_3$, $v_{CQ2} = v_{CQ3} = 0$. Since $i_{Lr1}(t_3)$ is positive, D_{Q2} and D_{Q3} are conducting and Q_2 and Q_3 turn on with zero-voltage switching after time t_3. Since Q_2, Q_3, D_2, and D_3 are conducting, $v_{ab} = -V_{in}$ and $v_{Lm1} = -nV_o$. C_{r1} and L_{r1} are naturally resonant with $v_{ab} = -V_{in}$ and $v_{Lm1} = -nV_o$. In step 4, i_{Lr1} and i_{Lm1} both decrease.

Step 5 [t_4 ~ t_5]: At time t_4, $i_{Lm1} = i_{Lr1}$, and D_1 ~ D_8 are off. Therefore, L_{r1}, C_{r1}, and L_{m1} are naturally resonant with $v_{ab} = -V_{in}$.

Step 6 [t_5 ~ $T_s + t_0$]: Q_2 and Q_3 turn off at t_5. Owing to $i_{Lr1}(t_5) < 0$, C_{Q1} and C_{Q4} are discharged. At time $T_s + t_0$, $v_{CQ1} = v_{CQ4} = 0$. Then, the circuit operations in a switching cycle are completed.

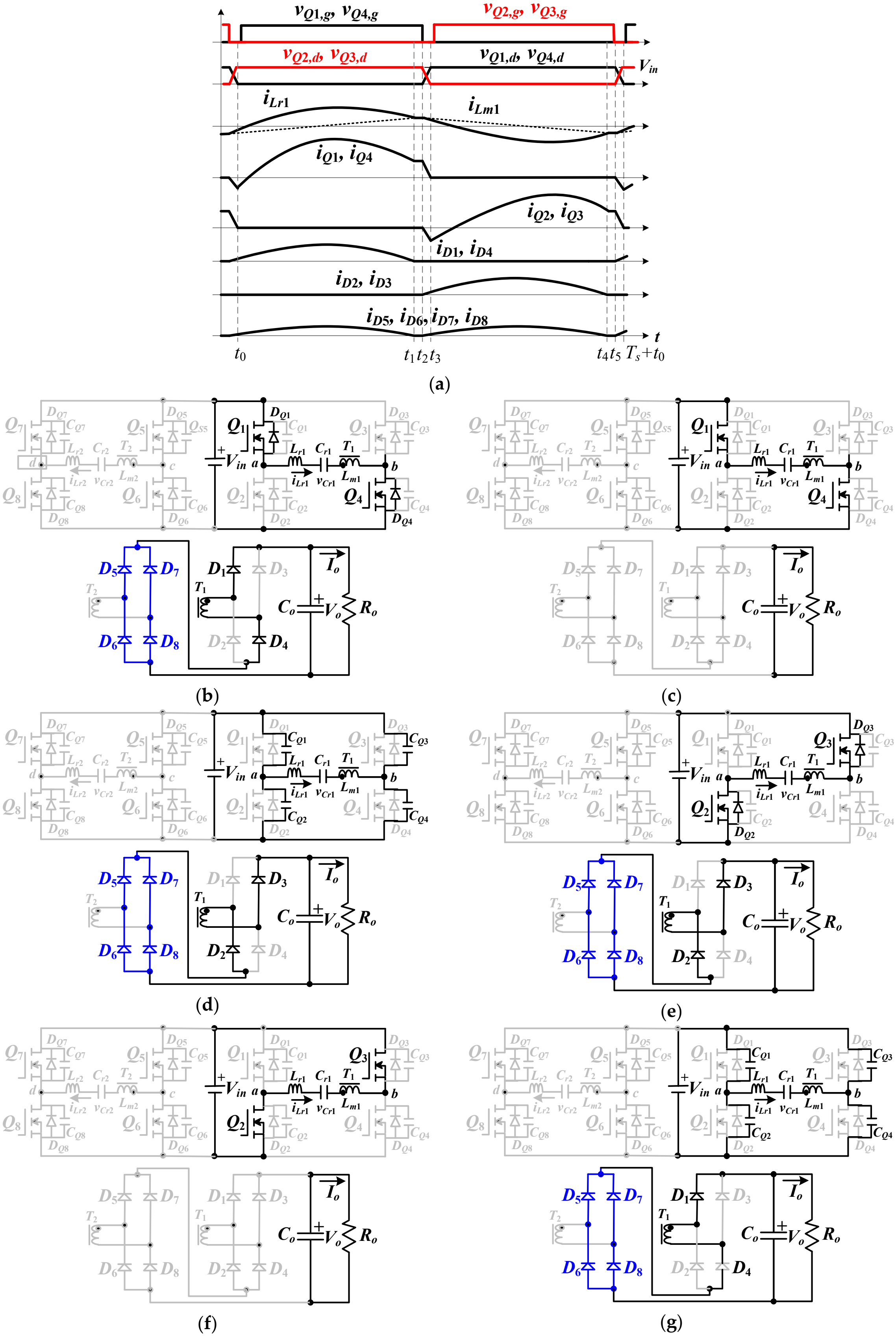

Figure 5. Circuit waveforms and equivalent circuits at high input voltage range and $f_s < f_r$, (**a**) PWM waveforms, (**b**) step 1, (**c**) step 2, (**d**) step 3, (**e**) step 4, (**f**) step 5, (**g**) step 6.

3. Circuit Analysis and Design Procedures

Variable frequency control is used to generate the PWM signals of power switches and regulate output voltage at V_o = 400 V under wide voltage variation from V_{in} = 100 V to 400 V. Then, a dc/ac inverter can be adopted as the second stage for PV inverter applications. The fundamental harmonic analysis is adopted to derive the voltage transfer function of the proposed converter. For low voltage input range from V_{in} = 100V to 200V, two resonant converters are operated, and the output voltages of two diode rectifiers are series connection to achieve high voltage gain (Figure 1b). For high voltage input range from V_{in} = 200 V to 400 V, only one resonant converter is operated on the primary side to regulate load voltage (Figure 1c). Since the frequency modulation is used in the presented circuit, it can obtain that the waveforms on v_{ab} and v_{cd} are square voltage waveforms. Based on the Fourier Series Analysis (FSA), the fundamental root-mean-square (*rms*) voltages $V_{ab,rms}$ and $V_{cd,rms}$ are obtained as.

$$V_{ab,rms} = 2\sqrt{2}V_{in}/\pi, \tag{2}$$

$$V_{cd,rms} = \begin{cases} 2\sqrt{2}V_{in}/\pi, 100\text{V} \leq V_{in} < 200\text{V} \\ 0, 200\text{V} < V_{in} \leq 400\text{V} \end{cases}, \tag{3}$$

For low input voltage range (V_{in} = 100 V ~ 200 V), the magnetizing voltages $v_{Lm1} = v_{Lm2} = \pm nV_o/2$. On the other hand, the magnetizing voltage $v_{Lm1} = \pm nV_o$ and $v_{Lm2} = 0$ for high input voltage range (V_{in} = 200 V ~ 400 V). Therefore, the fundamental *rms* magnetizing voltages are derived as.

$$V_{Lm1,rms} = \begin{cases} \sqrt{2}nV_o/\pi, \ 100\text{V} \leq V_{in} < 200\text{V} \\ 2\sqrt{2}nV_o/\pi, \ 200\text{V} < V_{in} \leq 400\text{V} \end{cases}, \tag{4}$$

$$V_{Lm2,rms} = \begin{cases} \sqrt{2}nV_o/\pi, 100\text{V} \leq V_{in} < 200\text{V} \\ 0, 200\text{V} < V_{in} \leq 400\text{V} \end{cases}, \tag{5}$$

According to the dc load resistor R_o, the equivalent ac resistors R_{ac1} and R_{ac2} on the primary-side of T_1 and T_2 can be obtained as:

$$R_{ac1} = \begin{cases} \frac{4n^2R_o}{\pi^2}, \ 100\text{V} \leq V_{in} < 200\text{V} \\ \frac{8n^2R_o}{\pi^2}, \ 200\text{V} < V_{in} \leq 400\text{V} \end{cases}, \tag{6}$$

$$R_{ac2} = \frac{4n^2R_o}{\pi^2}, \ 100\text{V} \leq V_{in} < 200\text{V}, \tag{7}$$

According to the resonant components L_{r1}, C_{r1}, $R_{ac1,}$ and L_{m1}, the voltage gain of the presented resonant converter is derived in (8).

$$|G| = \frac{V_{Lm1,rms}}{V_{ab,rms}} = 1/\sqrt{\left[1 + \frac{1}{l_n}\frac{f_n^2 - 1}{f_n^2}\right]^2 + x^2\left(\frac{f_n^2 - 1}{f_n}\right)^2} = \begin{cases} \frac{nV_o}{2V_{in}}, \ 100\text{V} \leq V_{in} < 200\text{V} \\ \frac{nV_o}{V_{in}}, \ 200\text{V} < V_{in} \leq 400V \end{cases}, \tag{8}$$

where $x = \sqrt{L_{r1}/C_{r1}}/R_{ac1}$ is the quality factor, $l_n = L_{m1}/L_{r1}$ is the inductor ratio, and $f_n = f_s/f_r$ is the frequency ratio. The output voltage can be obtained in (9).

$$V_o = \begin{cases} \frac{2V_{in}}{n\sqrt{\left[1+\frac{1}{l_n}\frac{f_n^2-1}{f_n^2}\right]^2 + x^2\left(\frac{f_n^2-1}{f_n}\right)^2}}, \ 100\text{V} \leq V_{in} < 200V \\ \frac{V_{in}}{n\sqrt{\left[1+\frac{1}{l_n}\frac{f_n^2-1}{f_n^2}\right]^2 + x^2\left(\frac{f_n^2-1}{f_n}\right)^2}}, \ 200\text{V} < V_{in} \leq 400V \end{cases} \tag{9}$$

According to the input and output voltage conditions, the switching frequency of power switches $Q_1 \sim Q_8$ are regulated according to the input voltage variation. Since the input impedance of the proposed resonant circuit is controlled at the inductive load, $Q_1 \sim Q_8$ can be turned on under zero voltage switching. The power loss analysis of the resonant converter or inverters has been discussed in [17,18] for fixed switching frequency. However, the switching frequency of the resonant converter is variable. Therefore, it is very difficult to predict and calculate the actual power losses. In the proposed converter, the main power losses are conduction losses on power switches $Q_1 \sim Q_8$, copper and core losses on the resonant inductors L_{r1} and L_{r2} and transformers T_1 and T_2, conduction losses on the resonant capacitors C_{r1} and C_{r2}, and the conduction losses on the rectifier diodes $Q_1 \sim Q_8$. The *rms* currents of the resonant capacitors C_{r1} and C_{r2} at the series resonant frequency are calculated as:

$$i_{Cr1,rms} = i_{Cr2,rms} = i_{Lr1,rms} = i_{Lr2,rms} \approx \sqrt{\left(\frac{\pi I_o}{2n\sqrt{2}}\right)^2 + \left(\frac{V_{Lm1}}{4\sqrt{3}L_{m1}f_{sw}}\right)^2}, \quad (10)$$

It is clear that the primary currents are related to the switching frequency f_{sw} and the magnetizing voltage V_{Lm1}. In the same input voltage range such as V_{in} = 100 V ~ 200 V, the low input voltage (V_{in} = 100 V) will result in low switching frequency. The low switching frequency will increase the primary current and conduction loss on power switches, inductors, and resonant capacitors. Therefore, the proposed converter efficiency at V_{in} = 100 V is less than the efficiency at V_{in} = 200 V. For low input voltage range (V_{in} = 100 V ~ 200 V), two resonant circuits are operated, and the magnetizing voltages $V_{Lm1} = V_{Lm2} = nV_o/2$ instead of $V_{Lm1} = nV_o$ under high input voltage range (V_{in} = 200 V ~ 400 V). Therefore, the circuit efficiency operated at low input voltage range is better than the circuit efficiency operated at high input voltage range.

To confirm the theoretical analysis, a design example of a laboratory circuit is provided with the electric specifications V_{in} = 100 V ~ 400 V and V_o = 400 V. The rated power is 1800 W (by two resonant circuits) for low input voltage range and 1 kW (by one resonant circuit) for high input voltage range. The series resonant frequency of the resonant tank is designed at 100 kHz. For low input voltage range V_{in} = 100 V ~ 200 V, two resonant circuits with parallel-series connection are operated in the studied circuit to obtain high voltage gain. However, one only resonant circuit is operated under high voltage input V_{in} = 200 V ~ 400 V. Figure 6 provides the voltage gain of the studied converter with wide input voltage operation. The transient voltage ($V_{in,tran}$) between low input voltage range and high input voltage range is selected at 200 V with ±4 V voltage tolerance. From equation (8), it is clear that the voltage gain of the presented resonant converter under high input voltage range is two times of voltage gain under low input voltage range. Therefore, the design considerations for two resonant converters operation (Figure 1b) for low voltage input and one resonant converter operation (Figure 1c) for high voltage input are identical. To simplify the design consideration, only one resonant converter under high voltage range is discussed to design circuit components. Under high voltage range, the minimum voltage gain G_{min} is designed as unity at $V_{in,max}$ = 400 V. From equation (8), the turn-ratio n_1 is obtained as:

$$n = n_1 = n_2 = \frac{G_{\min}V_{in,\max}}{V_o} = \frac{1 \times 400}{400} = 1, \quad (11)$$

Magnetic cores EE-55 with flux density ΔB = 0.4 *tesla* and window area A_e = 3.54 cm^2 are used to build the isolated transformers T_1 and T_2. The minimum switching frequency of the resonant converter is designed at 55 kHz and 200 V input. Therefore, the minimum primary turns at 200 V input are calculated as:

$$N_{p1,\min} \geq \frac{nV_o}{f_{s,\min}\Delta BA_e} = \frac{1 \times 400}{55000 \times 0.4 \times 3.54 \times 10^{-4}} \approx 51.4, \quad (12)$$

The actual primary turns and secondary turns of transformers T_1 and T_2 are $N_{p1} = N_{p2} = N_{s1} = N_{s2}$ = 52 turns. From equation (6), the equivalent resistance R_{ac1} under P_o = 1 kW and V_o = 400 V is obtained as:

$$R_{ac1} = \frac{8n^2}{\pi^2} R_{o,rated} = \frac{8 \times 1^2}{\pi^2} \times \frac{400^2}{1000} \approx 130\Omega, \tag{13}$$

The selected inductor ratio l_n is equal to 5, and the selected quality factor x is equal to 0.2. Based on the l_n, R_{ac1}, x, and f_r, the theoretical resonant components are derived as:

$$L_{r1} = L_{r2} = \frac{xR_{ac1}}{2\pi f_r} = \frac{0.2 \times 130}{2\pi \times 100 \times 10^3} \approx 41.4\mu H, \tag{14}$$

$$C_{r1} = C_{r2} = \frac{1}{4\pi^2 L_{r1} f_r^2} = \frac{1}{4\pi^2 \times 41.4 \times 10^{-6} \times (100 \times 10^3)^2} \approx 61nF, \tag{15}$$

$$L_{m1} = L_{m2} = l_n L_{r1} = 41.4 \times 5 = 207\mu H, \tag{16}$$

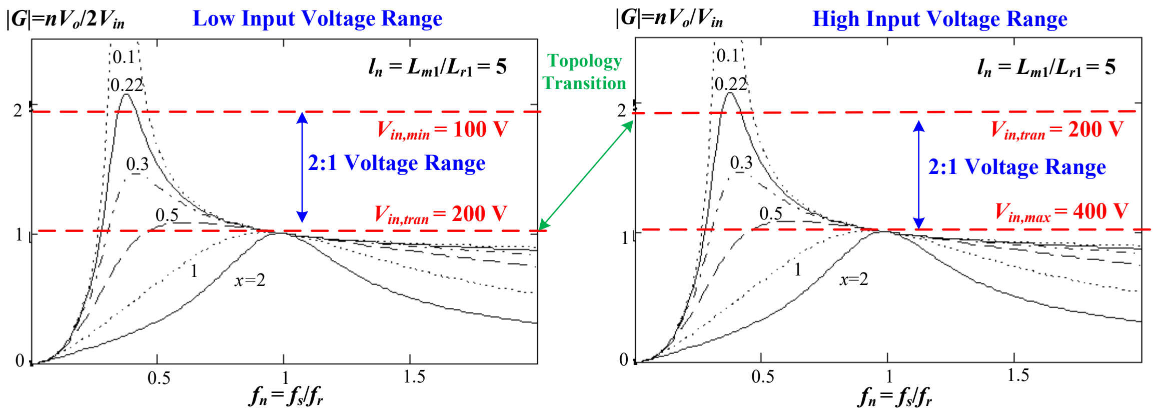

Figure 6. Voltage gain of the studied circuit for V_{in} 100 V ~ 400 V and V_o = 400 V.

In the prototype circuit, the actual resonant components are $L_{r1} = L_{r2}$ = 40 µH, $L_{m1} = L_{m2}$ = 200 µH and $C_{r1} = C_{r2}$ = 63 nF. The voltage stress of Q_1 ~ Q_8 equals $V_{in,max}$ = 400 V and power MOSFETs STW48N60M2 with 600 V/26 A rating are used for Q_1 ~ Q_8. The voltage stress of D_1 ~ D_8 equals V_o = 400 V and STTH8R06FP with 600 V/8 A are used for D_1 ~ D_8. The selected output capacitance C_o = 810 µF (three 270 µF in parallel).

4. Test Results

Experiments based on a prototype circuit shown in Figure 7 are demonstrated to confirm the circuit performance. The test results at low input voltage range are shown in Figures 8 and 9 with V_{in} = 100 V and 190 V, respectively. For low voltage range, two resonant circuits are operated with parallel-input and series-output structure to achieve high voltage gain. Figure 8 are the test waveforms under V_{in} = 100 V, V_o = 400 V and P_o = 1.8 kW. Figure 8a provides the measured waveforms of $v_{Q1,g}$ ~ $v_{Q8,g}$. The test switching frequency at V_{in} = 100 V shown in Figure 8a is about 51 kHz. Figure 8b gives the experimental waveforms of the resonant currents and voltages. Due to f_s (51 kHz) < f_r (100 kHz), the resonant currents i_{Lr1} and i_{Lr2} are quasi-sinusoidal waveforms. Figure 8c,d provide the current waveforms of the rectifier diodes. Owing to $f_s < f_r$, the rectifier diodes D_1 ~ D_8 are all reverse biased without reverse recovery current loss. Figure 8e demonstrates the experimental waveforms under V_{in} = 100 V, V_o = 400 V and I_o = 4.5 A (P_o = 1.8 kW). Figure 8f demonstrates the experimental waveforms of power switch Q_1 at full load. Before Q_1 turns on, the drain voltage $v_{Q1,d}$ is already zero voltage. Therefore, the zero voltage turn-on of Q_1 is achieved. Q_2 ~ Q_8 have the same turn-on characteristic as Q_1 with soft switching operation. Figure 9 provides the test waveform under V_{in} = 190 V, V_o = 400 V and P_o = 1.8 kW. The switch signals of Q_1 ~ Q_8 are provided in Figure 9a. The measured resonant current and voltages are given in Figure 9b. Since $f_s \approx f_r$, the resonant currents are sinusoidal waveforms. The measured diode currents are provided in Figure 9c,d. The measured waveforms of input voltage V_{in} = 190 V, load voltage V_o = 400 V and load current I_o = 4.5 A are provided in Figure 9e. The test waveforms of switch Q_1 are given in Figure 9f. For high input voltage range, Figures 10 and 11 shows the experimental results of the studied circuit at V_{in} = 210 V and 400 V, respectively. For high input voltage range, only one resonant converter (Q_1 ~ Q_4) is controlled to regulate load voltage. The rectifier diodes D_5 ~ D_8 are bypassed at high voltage range operation. The measured waveforms at V_{in} = 210 V, V_o = 400 V and P_o = 1 kW are provided in Figure 10. Due to the voltage gain at V_{in} = 210 V is close to 2 (under high input voltage range), it is obtained that $f_s < f_r$. From Figure 10b, the resonant current i_{Lr1} is a quais-sinusoidal waveform. From Figure 10c,d, D_1 ~ D_8 turn off under zero current switching. Since the diodes D_5 ~ D_8 are bypassed for high input voltage range, the secondary-side rectified current is distributed on D_5 ~ D_8. Therefore, the diode currents i_{D5} ~ i_{D8} are balanced and the amplitude of i_{D5} ~ i_{D8} is only one-half of amplitude of i_{D1} ~ i_{D4}. From test results in Figure 10f, it can observe that the soft switching turn-on of Q_1 is achieved. Figure 11 provides the test waveforms under V_{in} = 400 V, V_o = 400 V and P_o = 1 kW. The voltage gain at V_{in} = 400 V is 1 (Figure 6). The resonant current i_{Lr1} is a sinusoidal waveform (Figure 11b). Similarly, the secondary-side rectified current is distributed on D_5 ~ D_8 and the amplitude of i_{D5} ~ i_{D8} (Figure 11d) is equal to one-half of amplitude of i_{D1} ~ i_{D4} (Figure 11c). From the experimental waveforms in Figure 11f, Q_1 is turned on at zero voltage switching. The measured circuit efficiencies of the proposed converter are 92.55% at V_{in} = 100 V and P_o = 1.8 kW, 94.1% at V_{in} = 190 V and P_o = 1.8 kW, 90.8% at V_{in} = 210 V and P_o = 1 kW, and 91.8% at V_{in} = 400 V and P_o = 1 kW. It is clear that the proposed converter has better circuit efficiency at low input voltage case. Because the magnetizing current loss is depended on the output voltage instead of input voltage. For high voltage input, only one resonant converter is operated to provide 1 kW output. However, 1.8 kW is provided by two resonant converters at low voltage input case. Therefore, the proposed converter has better circuit efficiency at low input voltage case. Figure 12 provides the test circuit efficiencies of the proposed resonant converter for 50% and 100% rated power under different input voltages.

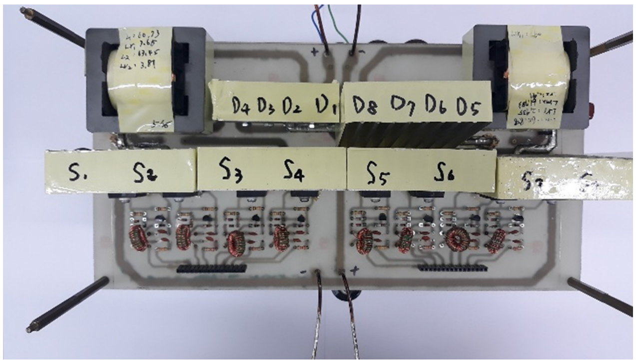

Figure 7. Picture of the laboratory prototype circuit.

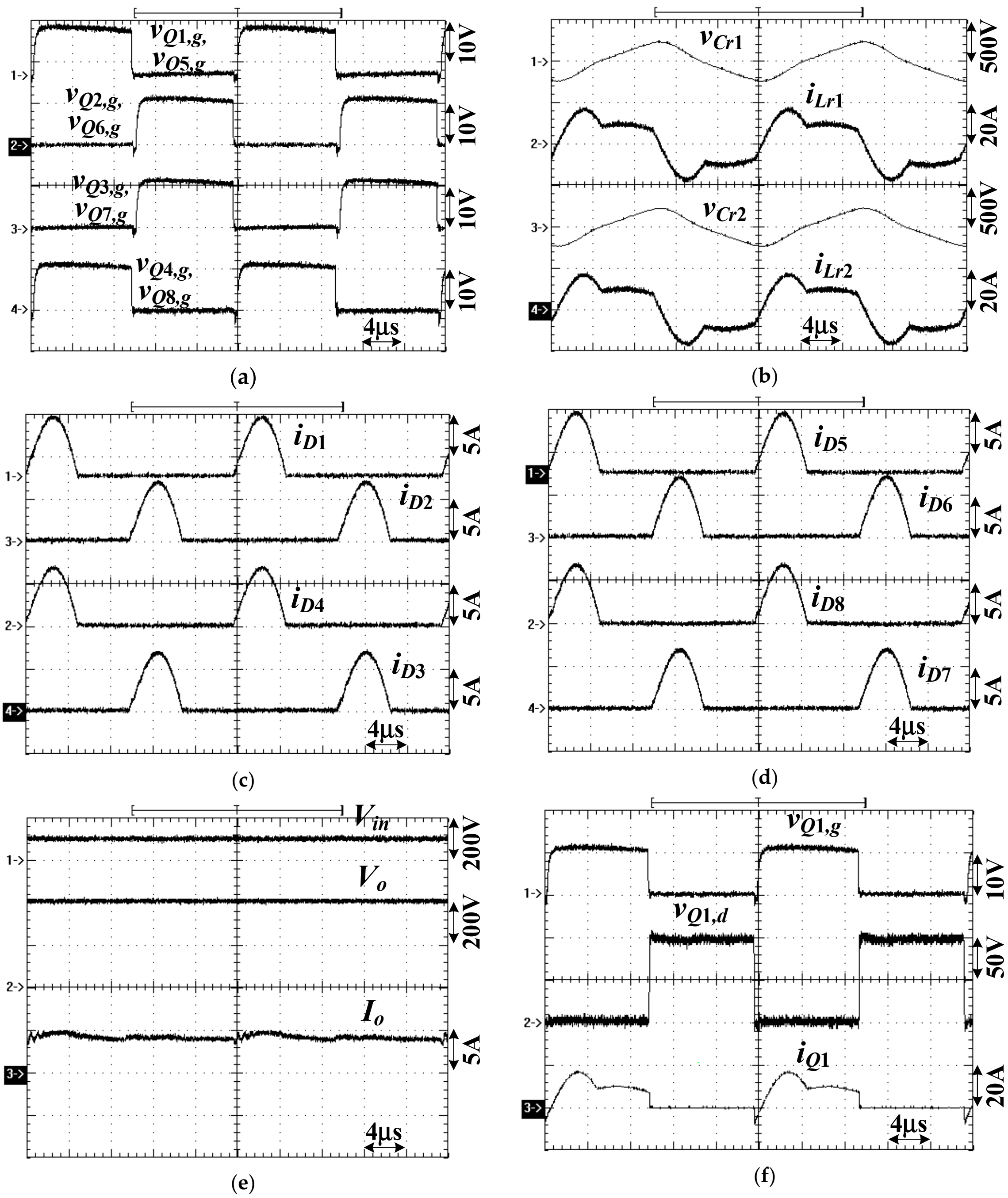

Figure 8. Experimental results at V_{in} = 100 V (low voltage range) and 1.8 kW load. (**a**) $v_{Q1,g}$ ~ $v_{Q8,g}$, (**b**) v_{Cr1}, i_{Lr1}, v_{Cr2}, i_{Lr2}, (**c**) i_{D1} ~ i_{D4}, (**d**) i_{D5} ~ i_{D8}, (**e**) V_{in}, V_o, I_o, (**f**) $v_{Q1,g}$, $v_{Q1,d}$, i_{Q1}.

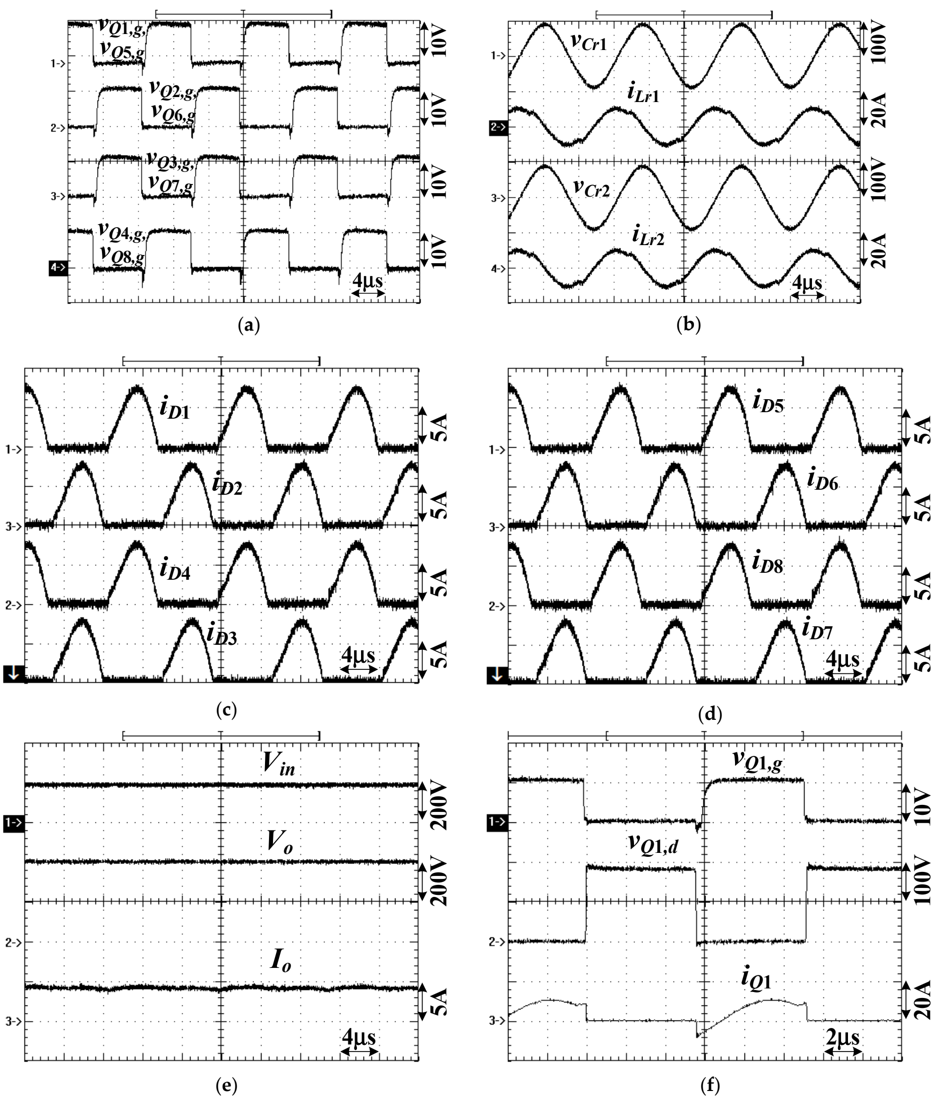

Figure 9. Experimental results at V_{in} = 190 V (low voltage range) and 1.8 kW load. (**a**) $v_{Q1,g}$ ~ $v_{Q8,g}$, (**b**) v_{Cr1}, i_{Lr1}, v_{Cr2}, i_{Lr2}, (**c**) i_{D1} ~ i_{D4}, (**d**) i_{D5} ~ i_{D8}, (**e**) V_{in}, V_o, I_o, (**f**) $v_{Q1,g}$, $v_{Q1,d}$, i_{Q1}.

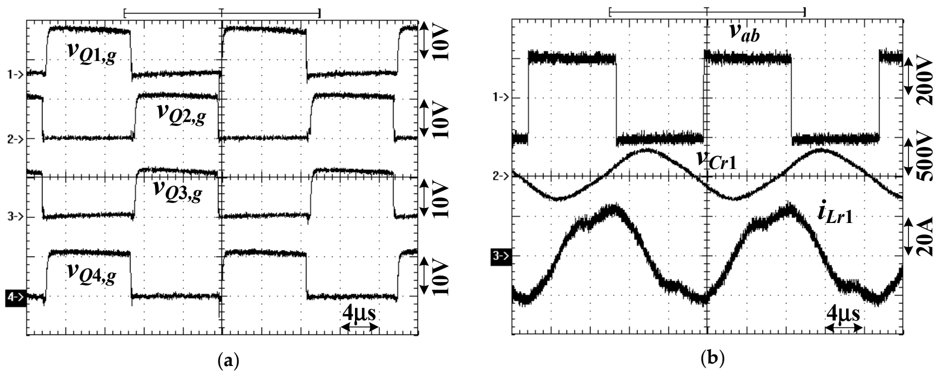

Figure 10. *Cont.*

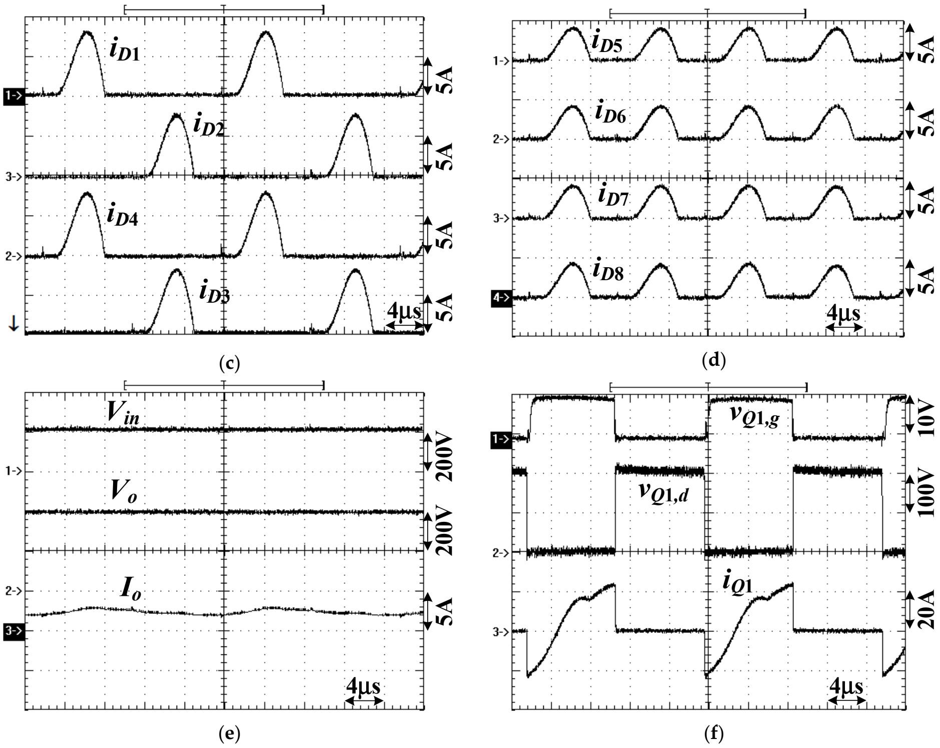

Figure 10. Experimental waveforms at V_{in} = 210 V (high voltage range) and 1 kW load. (**a**) $v_{Q1,g}$ ~ $v_{Q4,g}$, (**b**) v_{ab}, v_{Cr1}, i_{Lr1}, (**c**) i_{D1} ~ i_{D4}, (**d**) i_{D5} ~ i_{D8}, (**e**) V_{in}, V_o, I_o, (**f**) $v_{Q1,g}$, $v_{Q1,d}$, i_{Q1}.

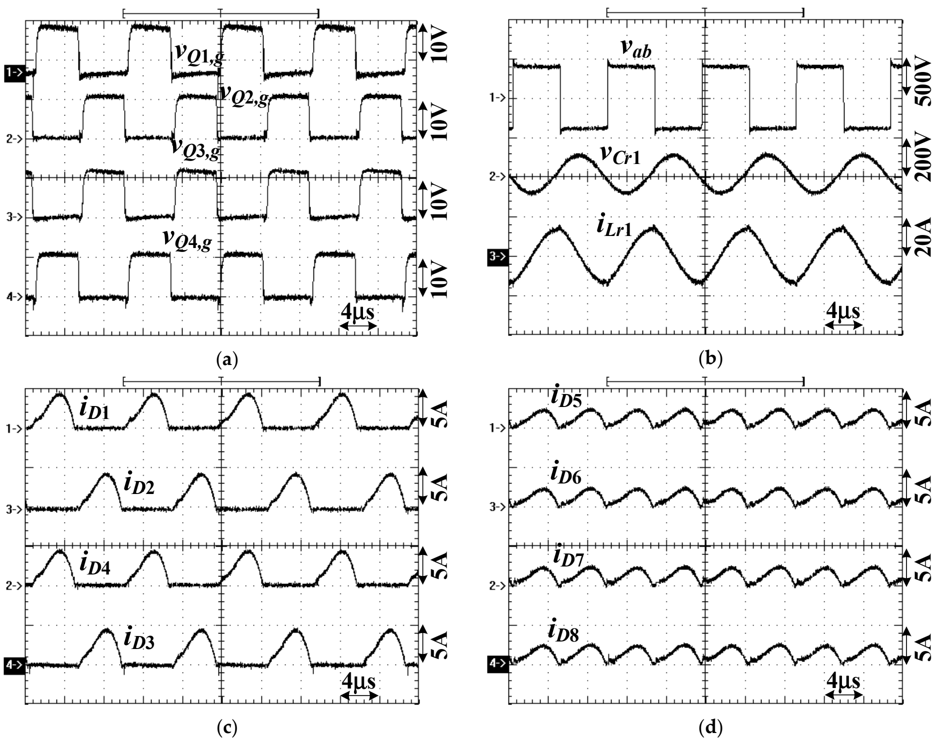

Figure 11. *Cont*.

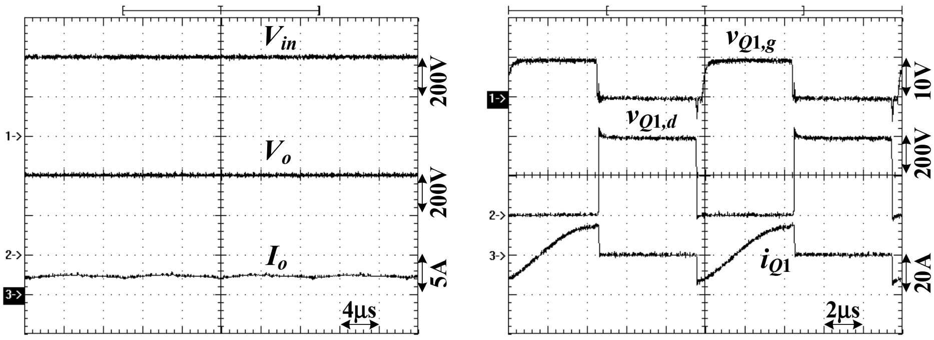

(e) (f)

Figure 11. Experimental results at V_{in} = 400 V (high voltage range) and 1 kW load. (**a**) $v_{Q1,g}$ ~ $v_{Q4,g}$, (**b**) v_{ab}, v_{Cr1}, i_{Lr1}, (**c**) i_{D1} ~ i_{D4}, (**d**) i_{D5} ~ i_{D8}, (**e**) V_{in}, V_o, I_o, (**f**) $v_{Q1,g}$, $v_{Q1,d}$, i_{Q1}.

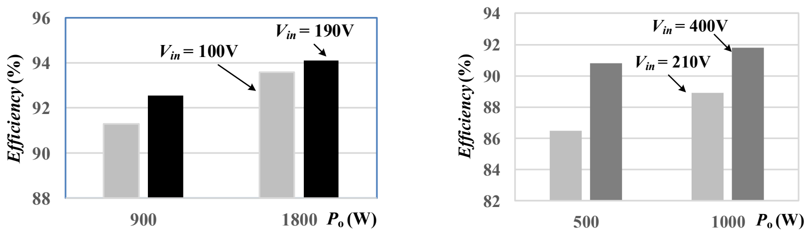

(a) (b)

Figure 12. Measured efficiencies of the proposed circuit for 50% and 100% rated power under different input voltages. (**a**) low input voltage range, (**b**) high input voltage range.

5. Conclusions

A new resonant converter is proposed, discussed, and implemented to have low switching losses on power devices and wide input voltage operation from V_{in} = 100 V to 400 V. To overcome the drawback of the limit range of input voltage operation on conventional resonant converter, two resonant circuits with parallel-series connection are used in the proposed converter. For low voltage input, the output voltages of two diode rectifiers are series-connected to have higher voltage gain. On the other hand, only one resonant circuit is operated and the other circuit is off under high input voltage range. Because the presented resonant circuit is operated at the inductive input impedance, the soft switching operation of all active devices is achieved. The proposed resonant converter can be implemented by the general integrated circuit with the frequency modulation and a voltage comparator. The applications of the studied circuit are front stage of solar power conversion with wide input voltage variation and high voltage output. Although two independent resonant converters working for each voltage range can also be adopted to achieve wide input voltage operation, the current rating of active and passive power components in the proposed converter is much lower (half current rating) than two converters working for low input voltage case. Finally, a 1.8 kW laboratory circuit was constructed and measured. Experiments are demonstrated to confirm the circuit performance and usefulness of the studied resonant converter with wide voltage range capability.

Author Contributions: B.-R.L. proposed and designed this project and was responsible for writing the paper.

Funding: This research is funded by the Ministry of Science and Technology, Taiwan, under grant number MOST 108-2221-E-224-022-MY2.

Acknowledgments: This research is supported by the Ministry of Science and Technology, Taiwan, under contract MOST 108-2221-E-224-022-MY2. The author would like to thank H. R. Cheng for his help to measure the circuit waveforms in the experiment.

Conflicts of Interest: The author declares no conflict of interest.

References

1. Wang, Y.; Zhang, S.; Guan, Y.; Liu, X.; Xu, D. Single-stage QR ac-dc converter based on buck-boost and flyback circuits. *IET Power Electron.* **2017**, *10*, 103–111. [CrossRef]
2. Xie, X.; Li, J.; Peng, K.; Zhao, C.; Lu, Q. Study on the single-stage forward-flyback PFC converter with QR control. *IEEE Trans. Power Electron.* **2016**, *31*, 430–442. [CrossRef]
3. Lin, B.R.; Chiang, H.K.; Chen, C.C. Analysis and implementation of a ZVS-PWM converter with series-connected transformers. *IEEE Trans. Circuits Syst. Part II Express Briefs* **2007**, *54*, 917–921. [CrossRef]
4. Singh, A.K.; Das, P.; Panda, S.K. Analysis and design of SQR-based high-voltage LLC resonant DC-DC converter. *IEEE Trans. Power Electron.* **2017**, *32*, 4466–4481. [CrossRef]
5. Haga, H.; Kurokawa, F. Modulation method of a full-bridge three-level LLC resonant converter for battery charger of electric vehicles. *IEEE Trans. Power Electron.* **2017**, *32*, 2498–2507. [CrossRef]
6. Lin, B.R.; Lin, Y. Parallel current-fed resonant converter with balance current sharing and no input ripple current. *IET Power Electron* **2019**, *12*, 212–219. [CrossRef]
7. Safaee, A.; Jain, P.; Bakhshai, A. A ZVS pulsewidth modulation full-bridge converter with a low-RMS-current resonant auxiliary circuit. *IEEE Trans. Power Electron.* **2016**, *31*, 4031–4047. [CrossRef]
8. Liu, P.J.; Hsu, Y.C.; Hsu, S.R. Drain-voltage balance and phase-shifted PWM control schemes for high-efficiency parallel-string dimmable LED drivers. *IEEE Trans. Ind. Electron.* **2018**, *65*, 6168–6176. [CrossRef]
9. Mishima, T.; Akamatsu, K.; Nakaoka, M. A high frequency-link secondary-side phase-shifted full-bridge soft-switching PWM DC-DC converter with ZCS active rectifier for EV battery charged. *IEEE Trans. Power Electron.* **2013**, *28*, 5758–5773. [CrossRef]
10. Zhang, Y.; Fu, C.; Sumner, M.; Wang, P. A wide input-voltage range quasi-Z-source boost DC–DC converter with high-voltage gain for fuel cell vehicles. *IEEE Trans. Ind. Electron.* **2018**, *65*, 5201–5212. [CrossRef]
11. Yao, Z.; Xu, J. A three-phase DC-DC converter for low and wide input-voltage range application. In Proceedings of the 2016 IEEE Transportation Electrification Conference and Expo, Asia-Pacific (ITEC Asia-Pacific), Busan, Korea, 1–4 June 2016; pp. 208–213.
12. Li, W.; Zong, S.; Liu, F.; Yang, H.; He, X.; Wu, B. Secondary-side phase-shift-controlled ZVS DC/DC converter with wide voltage gain for high input voltage applications. *IEEE Trans. Power Electron.* **2013**, *28*, 5128–5139. [CrossRef]
13. Wang, X.; Tian, F.; Batarseh, I. High efficiency parallel post regulator for wide range input DC–DC converter. *IEEE Trans. Power Electron.* **2008**, *23*, 852–858. [CrossRef]
14. Lu, J.; Kumar, A.; Afridi, K.K. Step-down impedance control network resonant DC-DC converter utilizing an enhanced phase-shift control for wide-input-range operation. *IEEE Trans. Ind. Applica.* **2018**, *54*, 4523–4536. [CrossRef]
15. Wu, H.; Wan, C.; Sun, K.; Xing, Y. A high step-down multiple output converter with wide input voltage range based on quasi two-stage architecture and dual-output *LLC* resonant converter. *IEEE Trans. Power Electron.* **2015**, *30*, 1793–1796. [CrossRef]
16. Hu, H.; Fang, X.; Chen, F.; Shen, Z.J.; Batarseh, I. A modified high-efficiency LLC converter with two transformers for wide input-voltage range applications. *IEEE Trans. Power Electron.* **2012**, *28*, 1946–1960. [CrossRef]
17. Albertoni, L.; Grasso, F.; Matteucci, J.; Piccirilli, M.C.; Reatti, A.; Ayachit, A.; Kazimierczuk, M.K. Analysis and design of full-bridge Class-DE inverter at fixed duty cycle. In Proceedings of the IECON 2016-42nd Annual Conference of the IEEE Industrial Electronics Society, Florence, Italy, 23–26 October 2016; pp. 5609–5614.
18. Ayachit, A.; Corti, F.; Reatti, A.; Kazimierczuk, M.K. Zero-voltage switching operation of transformer class-E inverter at any coupling coefficient. *IEEE Trans. Ind. Electron.* **2019**, *66*, 1809–1819. [CrossRef]